U-Th and [10]Be constraints on sediment recycling in proglacial settings, Lago Buenos Aires, Patagonia

Antoine Cogez[1], Frédéric Herman[1], Éric Pelt[2], Thierry Reuschlé[3], Gilles Morvan[2], Christopher M. Darvill[4], Kevin P. Norton[5], Marcus Christl[6], Lena Märki[1], and François Chabaux[2]

[1]University of Lausanne, Institut des Dynamiques de la Surface Terrestre, Quartier Unil-Mouline, Bâtiment Geopolis, CH-1015 Lausanne, Switzerland
[2]University of Strabourg, Laboratoire d'Hydrologie et de Géochimie de Strasbourg, Strasbourg, France
[3]University of Strabourg, Institut de Physique du Globe de Strasbourg, Strasbourg, France
[4]Geography Program and Natural Resources and Environmental Studies Institute, University of Northern British Columbia, 3333 University Way, Prince George, BC, V2N 4Z9, Canada
[5]Victoria Univeristy of Wellington, School of Geography, Environment, and Earth Sciences, Wellington, New Zealand
[6]Swiss Federal Institute of Zürich, Ion Beam Physics Laboratory, Zürich, Switzerland

Correspondence to: Antoine Cogez (antoine.cogez@gmail.com)

Abstract. The estimation of sediment transfer times remains a challenge to our understanding of sediment budgets and the relationships between erosion and climate. Uranium (U) and Thorium (Th) isotope disequilibria offer a means of more robustly constraining sediment transfer times. Here, we present new Uranium and Thorium disequilibrium data for a series of nested moraines around Lago Buenos Aires in Argentine Patagonia. The glacial chronology for the area is constrained using *in situ* cosmogenic [10]Be analysis of glacial outwash. Sediment transfer times within the periglacial domain were estimated by comparing the deposition ages of moraines to the theoretical age of sediment production, i.e. the comminution age inferred from U disequilibrium data and recoil loss factor estimates. Our data show first that the classical comminution age approach must include weathering processes, accounted for by measuring Th disequilibrium. Second, our combined data suggest that the pre-deposition history of the moraine sediments is not negligible, as evidenced by the large disequilibrium of the youngest moraines despite the equilibrium of corresponding glacial flour. Monte Carlo simulations suggest that weathering was more intense before the deposition of the moraines and that the transfer time of the fine sediments to the moraines was on the order of 100-200 ka. Long transfer times could result from a combination of long sediment residence times in the proglacial

lake (recurrence time of a glacial cyle) and the remobilization of sediments from moraines deposited during previous glacial cycles. [10]Be data suggest that some glacial cycles are absent from the preserved moraine record (seemingly every second cycle), supporting a model of reworking moraines and/or fluctuations in the extent of glacial advances. The chronological pattern is consistent with the U-Th disequilibrium data and the 100-200 ka transfer time. This long transfer time raises the question of the proportion of freshly eroded sediments that escape or not the proglacial environments during glacial periods.

1   Introduction

The sedimentary cycle incorporates the erosion of rocks followed by the transport and deposition of sediments. While rates of erosion and deposition can be accurately documented, tracing the history of sediments between production and deposition remains challenging. Importantly, mechanisms of transfer and alteration of sediments during transport play a key role in the evolution of basins and feedbacks between erosion and climate, especially because the age of sediment strongly controls its susceptibility to weathering (e.g. White & Brantley, 2003; Vance et al., 2009). This is particularly the case in glacial settings because glaciers are highly efficient at eroding landscapes (e.g. Hallet et al., 1996; Koppes & Montgomery, 2009) and produce highly-reactive and easily-weathered sediments (Anderson et al., 1997; White & Brantley, 2003; Anderson, 2005). Moreover, glaciers can create large overdeepenings that are subsequently filled with sediments isolated from interactions with surface processes. The efficiency of evacuating those sediments post-deposition is poorly known.

Silicate weathering is an important surface parameter for cooling climate over geologic and glacial-interglacial timescales because it consumes CO_2 (Ebelmen; Walker et al., 1981). But its role in controlling CO_2 concentrations and climate variations over glacial-interglacial cycles is contentious (Foster & Vance, 2006; Vance et al., 2009; Lupker et al., 2013; von Blanckenburg et al., 2015; Cogez et al., 2015). Understanding whether weathering varied over these cycles requires robust determinations of sediment transfer times.

For example, long transport times can cause a lag and/or a damping of the response of weathering to climate or erosion forcing and bias reconstructions of erosion and weathering intensity and variations through time.

Geochemical tools offer a means of measuring sediment transport times. Uranium series isotopes are particularly useful because the diversity of chemical elements in the radioactive decay chain (U, Th and Ra) leads to disequilibrium during surface process fractionation. Moreover, the half-lives of these isotopes range from 1,500 to 250,000 years, corresponding to sediment transport process times. The timescales of weathering processes have been particularly well documented using U-Th-Ra disequilibria in soil sediments and river waters (e.g. Ackerer et al., 2016; Chabaux et al., 2008, 2012, 2013; Dosseto & Schaller, 2016; Dosseto et al., 2010, 2012, 2014; Granet et al., 2010; Keech et al., 2013; Ma et al., 2013). An alternative approach uses the fine fraction of silicates to date the time since physical erosion of sediments (DePaolo et al., 2006, 2012). The method is based on the α-recoil of uranium during radioactive decay, triggering the loss of a fraction of the daughter isotopes compared to the parent in small ($\leq 50\mu$m) grains. The time since comminution can theoretically be estimated, despite difficulties and limitations discussed in previous studies (Maher et al., 2006; Lee et al., 2010; Handley et al., 2013a, b; Dosseto et al., 2010). However, this method only involves the ^{234}U/^{238}U ratio and so neglects the effect of chemical weathering and further reduction of grain size after comminution.

In this study, we sampled sequences of nested moraines around Lago Buenos Aires in Argentine Patagonia, which range in age from 0 to 1 Ma (Singer et al., 2004; Kaplan et al., 2005, e.g.). The aim was to constrain the pre-deposition history of sediments within the moraines. First we refined the deposition age of five of the moraines using *in situ* cosmogenic ^{10}Be exposure and depth profile dating. To constrain the sediment transport times, we used the comminution ages approach combined with ^{230}Th disequilibrium measurements. We show that taking weathering into account can help to resolve previous issues with the comminution ages methodology. Finally, we are able to estimate that the pre-deposition history of the fine sediment (4-50 μm) is likely on the order of 100-200 ka, including sediment recycling and chemical weathering in the proglacial system. Our findings have implications for the understanding of the couplings between erosion and climate.

2 Settings and methods

2.1 The Lago Buenos Aires moraines

Lago Buenos Aires in Argentina (Lago General Carreras in Chile) is a large proglacial lake, around 100 km long and 5-20 km wide, oriented east-west, at 46°S (Figure 5). The present climate of the area is temperate, with an average annual precipitation of 100 mm/yr and temperatures between 4 and 14 °C, producing open steppe vegetation. On the eastern edge of the lake, a series of frontal moraines are nested from the youngest close to the lake to the oldest 50 km further east. The chronology of these moraines has been studied: the five innermost moraines (Fenix 1-5) are Last Glacial Maximum (LGM) in age (Kaplan et al., 2004; Douglass et al., 2006). Singer et al. (2004) dated lava flows interbedded with six of the intermediary moraines (Moreno 1-3 and Deseado 1-3) and showed that they range in age between 109 ka and 760 ka. Finally, six moraines (Telken 1-6) in the outermost part of the system were likely deposited between 760 ka and 1016 ka. Mercer & Sutter (1982) showed that the oldest glaciogenic sediments we find in the area are 6 Ma, and consist of tills interbedded with lava flows that preserved them from erosion. Cosmogenic nuclide exposure dating of boulders supports the assertion that erosion and degradation of older moraines in this region yields erroneously young ages (e.g. Kaplan et al., 2005; Hein et al., 2009). Recently, Hein et al. (2017) used exposure dating of cobbles on outwash related to the Moreno moraines to show that they were constructed at ca. 260-270 ka, during Marine Isotope Stage (MIS) 8. For this study, we further refined the chronology by providing direct age constraints for the Deseado 1, Deseado 2 and Telken 5 moraines (see section 2.2).

U and Th samples were taken from silty beds inside the moraines, several meters below the surface in order to avoid potential post depositional modifications, such as weathering or dusts inputs (see picture in supplementary materials). In addition to moraine samples, a glacial flour sample was taken at the front of the Los Exploradores Glacier in Laguna San Rafael National Park to estimate the initial U-Th composition of silts found in the moraines (Figure 5). This glacier covers part of the total catchment draining into Lago Buenos Aires. Consequently, it is unlikely to be representative of the entire basin but provides an estimate of the initial composition of silts after comminution.

2.2 [10]Be methodology

2.2.1 Sampling

The cosmogenic nuclide exposure dating methodology followed the sampling recommendations of Hein
et al. (2009) and Darvill et al. (2015). We sampled quartzite cobbles for [10]Be analysis from the surfaces of
outwash grading to the Deseado 1, Deseado 2 and Telken 5 moraines. Similar samples were taken for Moreno
1 and 3 moraines and are presented in Hein et al. (2009). Using outwash cobbles has been shown to overcome
issues of post-depositional erosion that affects moraine boulders in this area (Hein et al., 2009), but relies on
finding locations where there is a clear geomorphic relationship between the glacial outwash and moraines.
At suitable locations, cobbles were targeted based on quartz composition, size (6-15 cm and 300-1,000
g to contain sufficient [10]Be), and preservation (sub-rounded shape, little aeolian erosion, partially buried
suggesting they were *in situ*). Surface lowering or up-freezing of cobbles can result in vertical movement
through the outwash unit. In this region, it is more likely that cobbles will underestimate the true age of the
unit (Hein et al., 2009; 2017). To circumvent this issue three or four cobbles were analysed at each sampling
location, and the oldest taken as the best estimate of moraine deposition age.

As well as cobbles from the outwash surfaces, [10]Be depth profiles through exposures within the outwash
units were used to estimate surface erosion rates and nuclide inheritance. We sampled through two outwash
profiles relating to the Deseado 2 and Telken 5 moraines. Each of the samples making up the depth profiles
consisted of 50 to 100 quartz-rich gravel clasts taken from horizontal lines, 2-4 cm wide at various depths
below the surface. Five depths were sampled per profile between 50 cm and 240 cm deep; sufficient depth
to account for nuclide attenuation from the surface and reliably estimate any cosmogenic [10]Be inheritance.
The top 50 cm of the profiles were carbonated due to post depositional processes but the rest of the profiles
were of relatively consistent density. See supplementary materials for pictures.

2.2.2 Analytical methods

Surface cobbles were analysed individually as independent estimates of exposure age. The gravels at each
depth in the profiles were amalgamated to produce an average nuclide concentration for that depth. Samples
were crushed and sieved to obtain the 125-250 μm and the 250-500 μm fractions, which were then purified
using a Frantz magnetic separator to isolate non magnetic fractions. Following dissolution in concentrated

HF, the residual sample material was leached with 10mL H_2O to extract $Be(OH)_2$ (Stone, 1998). A combination of anion and cation resins and precipitation was used to purify Be (von Blanckenburg et al., 2004; Norton et al., 2008). The oxidized BeO was mixed with Nb powder and pressed into cathodes and measured on the 0.5 MeV Tandy accelerator at ETH Zürich (Müller et al., 2010). The resulting $^{10}Be/^9Be$ ratios were normalized to S2007N ($^{10}Be/^9Be = 28.1 \times 10-12$; (Christl et al., 2013; Kubik & Christl, 2010)), with a ^{10}Be half-life of 1.387 ± 0.012 Ma (Chmeleff et al., 2010; Korschinek et al., 2010). Measured $^{10}Be/^9Be$ ratios were 30 - 500 times higher than the procedure blank ($9.60 \times 10^{-15} \pm 4.77 \times 10^{-15}$). Blank corrected ^{10}Be concentrations decrease exponentially with depth from greater than 36×10^5 for near surface samples to less than 2×10^5 at 2 meters depth.

2.2.3 Deposition ages calculations

Exposure ages for the outwash surface cobbles were calculated from ^{10}Be concentrations using version 2.3 of the CRONUS online calculator (Balco et al., 2008). Shielding was measured in the field (>0.999999 for every sample), a density of 2.65 $g.cm^{-3}$ was used for every sample, and no erosion rate was applied since there were no visible signs of surface erosion. We used the global ^{10}Be production rate of Borchers et al. (2016) (4 at/g/yr) and the 'Lm' scaling scheme (as described in Balco et al. (2008), Lal (1991) and Stone (2000) with paleomagnetic corrections from Nishiizumi et al. (1989)). However the scatter between the different scaling schemes is comparable to the external uncertainties. The production rate from Kaplan et al. (2011), calculated from a site very close to LBA, gives 3.6 at/g/yr (instead of 4 for Borchers et al. (2016)). The difference in calculated exposure ages between those two productions rates remains within uncertainties.

We modeled the most probable deposition age, surface erosion rate, and nuclide inheritance for each depth profile using the Monte Carlo simulation approach of Hidy et al. (2010). A site production rate of 6.2 atoms/g/yr was used, taken from an average of the scaling schemes in the CRONUS calculator. Changing this production rate by ±0.3 atoms/g/yr does not significantly alter the results. This range of site production rates (5.9-6.5 atoms/g/yr) corresponds to SLHL production rates 3.6-4 at/gr/yr, using the Lm scaling scheme. We used an average profile density of 2.5 $g.cm^{-3}$ (based on field observations), and a shielding factor of 1. The *a priori* values assigned to the Bayesian Monte Carlo simulation were: 0 to 1 cm/ka erosion rate with a maximum erosion threshold of 1000 cm and uniform distribution (based on erosion rates in Hein et al. (2009)

for the Hatcher profile in nearby Lago Pueyrredon and Darvill et al. (2015)); 0 to 10^5 atoms/g inheritance with uniform distribution (based on concentrations in the lower levels of the profiles); 200 to 800 ka age range for Deseado 2 and 700 to 1200 ka age range for Telken 5, with uniform distribution. These ages were chosen based on the argon ages of Singer et al. (2004) and the Moreno age refinement of Hein et al. (2017).

2.3 U-Th methodology

2.3.1 Principles and theory

U-Th series disequilibria were used since a few decades in order to determine time constant of weathering. We refer to the supplementary material for more references about it. The comminution age theory introduced by DePaolo et al. (2006) is a promising approach to estimating the age of sediment production. ^{238}U decays into ^{234}Th with a half life of 4.5 Ga. During this α emission, the daughter isotope recoils over a distance of several tens of nanometers depending on the type of mineral (e.g. 30 nm for a feldspar). ^{234}Th quasi instantaneously produces ^{234}U, with a longer half life of 245 ka: long enough to be measurable and usable on geologic timescales. If the ^{238}U decay occurs on the edge of a sediment grain, the daughter isotope is ejected from the grain and a disequilibrium in the decay chain starts as the ^{234}U/^{238}U ratio of the grain starts to decrease. If the grain is small enough, with a large surface area compared to its volume, the disequilibrium can be measured. Steady state is reached after a time characterized by the half life of ^{234}U. During this transient state, the magnitude of the disequilibrium in a grain equates to the time since it was produced. The steady state disequilibrium value depends on the fraction of ^{234}U ejected out of the grain due to α recoil. The process can be modeled using the following two equations describing the evolution of ^{238}U and ^{234}U:

$$\frac{dN_{238}}{dt} = -\lambda_{238} N_{238}$$

$$\frac{dN_{234}}{dt} = -\lambda_{234} N_{234} + (1 - f_\alpha^{234}) \lambda_{238} N_{238}$$

λ_{234} and λ_{238} are the decay constants of ^{234}U and ^{238}U respectively. N_{234} and N_{238} are the number of nuclides for each isotope, and f_α^{234} is the recoil loss fraction of ^{234}U (the proportion of ^{234}U in the grain ejected during α decays). This parameter is critical, since it represents the process whose existence determine the possibility of tracing the comminution age. When the effect of this process starts to be measurable, the clock starts. We discuss in more detail how this parameter can be evaluated in section 2.3.4. The evolution of the U/Th ratio over time is shown in Figure 3 (blue curves). The steady state disequilibrium model is based

on the assumption that the sediment grain has not been weathered over time, or at least that the loss of nuclide due to weathering was negligible compared to loss by α-recoil. The assumption may be valid for very arid areas, but is otherwise unlikely to hold true. However, the influence of weathering on the comminution age model has not been investigated.

5   In order to decouple the respective influence of α-recoil and weathering, we measured ^{230}Th concentration. The solubility of thorium is much lower than uranium. Therefore the ratio of ^{230}Th/^{234}U can inform weathering rates. ^{230}Th is produced by ^{234}U decay with a half life of 75 ka. It can also be ejected out of the grain due to α-recoil. The recoil loss fraction of ^{230}Th, $^{230}_{\alpha}$ is related to $^{234}_{\alpha}$ (Hashimoto et al., 1985; Neymark, 2011)

10    $$f_{\alpha}^{230} = f_{\alpha}^{234} \times \frac{\alpha_{230} M_{234}}{\alpha_{234} M_{230}} = 1.176 \times f_{\alpha}^{234} \tag{1}$$

α_{230} and α_{234} are the decay energy of ^{238}U to ^{234}U and of ^{234}U to ^{230}Th, respectively (71.79 and 82.96 keV respectively). M_{234} and M_{230} are the atomic mass of ^{234}U and ^{230}Th. This gives $f_{\alpha}^{230} = 1.176 \times f_{\alpha}^{234}$. (In practice f_{α}^{230} is probably larger since ^{234}U is on damaged sites, so it increases the probability for ^{230}Th to be ejected from the grain during a decay). The evolution of the number of nuclides ^{230}Th is then given by

15    $$\frac{dN_{230}}{dt} = -\lambda_{230} N_{230} + (1 - f_{\alpha}^{230}) \lambda_{234} N_{234} \tag{2}$$

Since $f_{\alpha}^{230} > f_{\alpha}^{234}$ and $\lambda_{230} > \lambda_{234}$, (^{230}Th/^{238}U) < (^{230}Th/^{234}U) < (^{234}U/^{238}U) is always verified. However, weathering would increase the ratio of ^{230}Th/^{234}U and ^{230}Th/^{238}U because Th is less soluble than U, and likely decrease the ratio of ^{234}U/^{238}U because radioactive decay places ^{234}U on a more fragile site compared to ^{238}U so that it could be more easily weathered (DePaolo et al., 2012; Handley et al., 2013a).
20   Consequently, Th isotopes can help to identify and quantify the effects of α-recoil and weathering, respectively. New equations can be derived for the evolution of the different nuclide contents following Chabaux et al. (2003, 2008), and Dosseto et al. (2008); Dosseto & Schaller (2016) :

$$\frac{dN_{238}}{dt} = -k_{238}N_{238} - \lambda_{238}N_{238}$$
$$\frac{dN_{234}}{dt} = -k_{234}N_{234} - \lambda_{234}N_{234} + (1 - f_\alpha^{234})\lambda_{238}N_{238}$$
$$\frac{dN_{230}}{dt} = -k_{230}N_{230} - \lambda_{230}N_{230} + (1 - f_\alpha^{230})\lambda_{234}N_{234}$$

where k_{238}, k_{234} and k_{230} are the leaching coefficient of ^{238}U, ^{234}U and ^{230}Th respectively. The solution is shown in figure 3.

The steady state activity ratios can also be derived:

$$\left(^{234}U/^{238}U\right)_{steady} = \frac{\lambda_{234}\left(1 - f_\alpha^{234}\right)}{\lambda_{234} + k_{234} - k_{238}}$$

$$\left(^{230}Th/^{234}U\right)_{steady} = \frac{\lambda_{230}\left(1 - f_\alpha^{230}\right)}{\lambda_{230} + k_{230} - k_{238}}$$

$$\left(^{230}Th/^{238}U\right)_{steady} = \frac{\lambda_{230}\lambda_{234}\left(1 - f_\alpha^{230}\right)\left(1 - f_\alpha^{234}\right)}{\left(\lambda_{230} + k_{230} - k_{238}\right)\left(\lambda_{234} + k_{234} - k_{238}\right)}$$

Here, parentheses are used to represent activity ratios, corresponding to the isotopic ratio multiplied by the ratio of the respective decay constants of each isotope.

2.3.2 Sample preparation

Silt samples were collected from moraines. Water has likely percolated through these silts since moraine deposition, triggering the precipitation of secondary carbonates, oxides, organic matter and clays. These secondary fractions have different U and Th disequilibria than the primary silicate and it is therefore important to remove them before analysis without altering the primary silicate fraction. We used the protocol established by Lee (2009), with slight modifications to help overcome the low solubility of Th that can make it difficult to remove during successive leaching, and allow Th to adsorb onto mineral surfaces after ejection from the grain. Our protocol is as follows:

1) The samples were sieved at 50 μm in order to collect the $\leq$ 50 μm fraction.

2) Approximately 10 g of this fraction was then weighed in a quartz crucible and heated for 4 hours at 550°C to burn organic matter. Lee (2009)'s optimal protocol uses H_2O_2 to dissolve organic matter, but other studies have shown that this reagent is not always fully selective (Tessier et al., 1979). The ashing of organic

matter yields similar results, but is normally conducted at the end of the procedure (Lee, 2009). By ashing first, we were able to process larger amounts of silt, limiting furnace contamination and aiding the process of dissolving of precipitates (mainly oxides formed during heating) in the following steps. Oxides turn the samples a brown to reddish color.

5   3) Sample grains were dispersed in 0.1 N sodium oxalate and the ≤ 4 μm fraction was removed using Stokes settling. The ≤ 4 μm fraction consists of clays and also primary silicates with larger U-Th disequilibria.

4) For each sample, 4 g of sediment was weighed in a 50 mL centrifuge tube and leached twice with 32 mL 1M magnesium nitrate to remove the exchangeable fraction and any residues of the ashing process.

10   5) 32 mL of acetic acid buffered to pH5 with 1M sodium acetate was then added and agitated at room temperature during 5 hours to dissolve the carbonates.

6) 40 mL of 0.04M hydroxilamine hydrochlorid in 25% (v/v) acetic acid was added and heated at 95°C for 6 hours twice over to dissolve oxides. After this procedure, the samples still had a brown to reddish color from oxides formed in the furnace. These amorphous oxides can be resistant to the hydroxylamine

15   hydrochloride treatment, as shown by Gontier (2014). These authors recommended using oxalic acid in ammonium oxalate (agitated in the dark at room temperature for 4 hours) (Leleyter & Probst, 1999). This procedure preserves silicate from dissolution (Gontier, 2014). Note that for the last three steps, the leaching residues were centrifuged and rinsed twice with mQ water.

At this stage the samples should contain only primary silicates between 4 and 50 μm. To evaluate whether

20   sample preparation fully removed secondary phases (e.g. carbonates, oxides, clays) without affecting primary silicates, we made Scanning Electron Microscopy (SEM) images at the University of Strasbourg, shown in section 3.2. Our observations showed the method to be effective (see the Supplementary Information for further discussion on the efficacy of Th removal in this protocol) and the samples were deemed ready for disequilibrium analysis.

25   Two duplicates of this pretreatment protocol were measured (see Table 3). They are remarkably consistent within errors for (^{230}Th/^{238}U) and (^{230}Th/^{234}U) and only slightly different for (^{234}U/^{238}U) (only twice the external uncertainty). Since the surface area data are also slightly different, this small difference could be associated with heterogeneities in the powder, or fractionation of the grain size during the sampling of the powder, or biases in the leaching process.

2.3.3 U-Th disequilibrium analysis

A first aliquot of the samples was dedicated to U-Th analysis. This aliquot was powdered in an agate ball mill to optimize sample homogeneity and acid dissolution. Approximately 100 mg of this powder was spiked with ^{233}U-^{229}Th tracer and digested with concentrated HF-HNO$_3$-HClO$_4$ acids following Pelt et al. (2013).

Separation and purification of U and Th followed standard anionic resin chromatography (Dequincey et al., 2002; Granet et al., 2007; Pelt et al., 2008). U and Th isotopic ratios and concentrations were determined by standard-sample bracketing (SSB) using an MC-ICPMS Neptune, following an optimised procedure upgraded from previously published protocols (Pelt et al., 2008; Ma et al., 2012; Bosia et al., 2016). The ^{233}U-^{229}Th spike was calibrated against the gravimetric NIST SRM 3164 and 3159 U and Th pure solutions. IRMM-184 and IRMM-035 isotopic standard solutions were spiked and used as bracketing solutions for U and Th SSB analysis, with the ^{233}U/^{234}U and ^{229}Th/^{230}Th ratios of these mixtures calibrated by TIMS Triton. We used the consensus value from Sims et al. (2008) for the ^{232}Th/^{230}Th ratio of the IRMM-035 standard and our own absolute TIMS Triton measurements for the ^{234}U/^{238}U ratio of the IRMM-184 standard instead of the certified values. The peak-tailing of the ^{232}Th over the ^{230}Th was corrected using an exponential law fitted by signals measured in 229.6 and 230.6 masses. The precision and accuracy of the data were estimated from regular analysis of international pure solutions (HU1 for (^{234}U/^{238}U): 1.0008±0.0005 (2σ, N=5), IRMM-036 for ^{232}Th/^{230}Th: 329064±1313 (2σ, N=5)) and rock basalts (BCR-2, AThO and BE-N). Results are consistent with published data and the ^{238}U-^{234}U-^{230}Th secular equilibrium assumed for old (several Ma) BCR-2 and BE-N 'unweathered' basalts, within errors. Based on these pure solutions and homogeneous basalt powders we estimate an uncertainty (2SD) of 0.2% for (^{234}U/^{238}U), 0.5-1% for (^{230}Th/^{232}Th) and 1-1.5% for (^{238}U/^{232}Th), (^{230}Th/^{238}U) and (^{230}Th/^{234}U). A duplicate of the protocol was measured and agree within the internal measurement uncertainties for (^{234}U/^{238}U), (^{230}Th/^{238}U), (^{230}Th/^{234}U) (see Table3). Usual blanks in the lab are in the range of 20-50 pg for U and 100-200 pg for Th and therefore negligible here.

2.3.4 Estimation of the recoil loss factor

The recoil loss parameter (f_α) is a critical parameter in comminution age theory as presented in section 2.3.1. Different methods have been proposed to estimate this parameter, summarized in Maher et al. (2006) and

Lee et al. (2010), but discrepancies up to an order of magnitude can be found between the different methods (Handley et al., 2013a, b). Here we used the N_2 gas absorption technique, which consists of surface area and fractal dimension measurements. Other methods are more subjective in that they involve visual estimation and assumptions for the aspect ratio and surface roughness coefficient. We measured the specific surface area for all samples and assessed the efficiency of this method to determine f_α and the relation between f_α and U-Th disequilibria.

A second aliquot of the samples (at least 1 g per sample) was prepared for these analyses, conducted at the Institut de Physique du Globe de Strasbourg on a Carlo Erba Sorptomatic 1990 machine. Details of the procedure are given in the Supplementary Information. Fractal dimension were also measured for each sample and the recoil loss factor f_α calculated following Bourdon et al. (2009), after Semkow (1991):

$$f_\alpha = \frac{1}{4}\left[\frac{2^{D-1}}{4-D}\left[\frac{a}{R}\right]^{D-2}\right] R.S.\rho_s \tag{3}$$

Where S is the specific surface area, D is the fractal dimension, a is the diameter of the adsorbate molecule (0.35 nm), R is the recoil lenght (30 nm), and ρ_s is the density of the solid (2650 kg.m^{-3}).

2.3.5 Determination of the recycling time and weathering intensities : Monte Carlo analysis

A Monte Carlo approach was used to determine weathering intensities during both the pre- and post-deposition histories of the different moraine silts, and the duration of this pre-deposition history (called 'recycling time' from this point forward).

[10]Be exposure ages inform on the deposition age of the moraines. The age extracted from U-Th data inform on the time since the sediment has been produced. So it is equal to the sum of sediment recycling time (time elapsed between commminution and deposition of the moraine) and the deposition age. The problem as formulated in section 2.3.1 has a large number of unknowns compared to the number of data in each equation. So the problem is underdetermined. However if geomorphology and climate did not vary too much between each glacial period, we can assume that recycling times and weathering intensities are comparable between the different sample. In facts, the glacial maxima observed since the Mid Pleistocene Transition are quite comparable. We can then assume that the processes (especially weathering) occuring during a glacial cycle are comparable in intensity from a cycle to another. Regarding the recycling time, the main

other parameter (apart from climate) influencing it is the morphology (mainly valleys and overdeepening). The Great Patagonian Glaciation oocured before 1 Ma (Mercer & Sutter, 1982), these glaciations are most probably responsible for carving the U shaped valleys and the overdeepening in which the lake is nowadays. Moreover the results of the numerical experiments of Kaplan et al. (2009), about the extent of ice related to the elevation of the accumulation area and the depth of the overdeepening, suggest that this overdeepening was most probably already carved before 1 Ma. Moreover, recently Christeleit et al. (2017) argued using thermochronometric data that the relief of Patagonia at the latitudes of our study was probably achieved between 10 and 5 Ma. On that basis, one can assume that the recycling time probably remained constant over the period covered by the samples. Hence the recycling time and weathering coefficients are considered the same between the different samples.

We used the theoretical scheme described in section 2.3.1 to estimate these weathering intensities and recycling time. Known or informed parameters in the Monte Carlo simulations were the activity ratios (^{234}U/^{238}U) and (^{230}Th/^{238}U), initial activity ratio (from the glacial flour sample), recoil loss factor f_α and deposition ages of the moraines (the post-depositional duration). Unknown parameters were the weathering intensities of ^{238}U, ^{234}U and ^{230}Th for the pre- and the post-deposition history. The relative weathering intensity of ^{234}U compared to ^{238}U, and ^{230}Th compared to ^{238}U, were assumed to be the same before and after moraine deposition. Consequently, we needed to determine five unknowns: the respective weathering coefficients k_{238}^{pre}, k_{238}^{post}, k_{234}/k_{238}, k_{230}/k_{238} and the recycling time t_{recycl} using Monte Carlo simulations. We chose a large, arbitrary number of values for the unknowns and calculated the activity ratios associated with these set of values. Then, we calculated a misfit M for the data as the difference between measured and modeled values, weighted by the uncertainty. The lower the misfit, the larger the probability of this set of values (we show the likelihood L for better visibility):

$$M = (m-o)^T \sigma^{-1} (m-o)$$

$$L = \exp(-M/2)$$

Where m is the vector of modeled parameters (the five unknowns above), o is the observed values (the activity ratios (^{234}U/^{238}U) and (^{230}Th/^{238}U)), and σ is the diagonal matrix of uncertainties on the data. In theory, an optimal solution can be determined, corresponding to the lower misfit (larger likelihood). However, no solutions were found because the number of unknowns was too great. We also know the relative weathering intensities of ^{238}U, ^{234}U and ^{230}Th : since Th is less soluble than U and ^{234}U is on more fragile

mineralogic sites. Hence, k_{230} is lower than k_{238}, and k_{234} is slightly larger than k_{238}. This information was used to further constrain the Monte Carlo simulations. For different couples of k_{234}/k_{238} and k_{230}/k_{238}, we ran a Monte Carlo optimization to find an optimal solution (lower misfit). All optimal solutions for k_{238}^{pre}, k_{238}^{post} and the recycling time are shown in Figure 6, and we use the optimal solutions to characterize the

5   pre-depositional duration of these sediments.

To test whether exchangeable Th might not be efficiently leached by our chemical protocol, we also made a simulation with $f_\alpha^{230} = 0$ and $f_\alpha^{230} = \dfrac{1.176 \times f_\alpha^{234}}{2}$ (half of the theoretical value described in section 2.3.1). If Th was totally readsorbed onto the mineral surfaces after ejection from the grain (and not subsequently removed during leaching), then it is equivalent to having no ejection ($f_\alpha^{230} = 0$). The case with $f_\alpha^{230} =$

10    $\dfrac{1.176 \times f_\alpha^{234}}{2}$ is an intermediary between total removal of the adsorbed Th and no removal at all, discussed further in the Supplementary Information.

3   Results

3.1   Cosmogenic [10]Be and deposition ages

The results of [10]Be analyses are shown in Figure 2 and Tables 2 and 1. Refer to supplementary information

15   for more details on the profiles ages results.

Eight surface cobbles from outwash relating to the Moreno 1 and 3 moraines yielded [10]Be exposure ages ranging from 168-269 ka (published in Hein et al. (2017)). To these we add six more surface exposure ages and two depth profile ages from outwash related to the Deseado and Telken moraines. Three cobbles from Deseado 1 produced relatively tightly-clustered exposure ages of 430-468 ka. A cobble from the ice-distal

20   Deseado 2 outwash yielded a much younger, stratigraphically-inconsistent age of 293 ka (sample D2-T12), similar to the Moreno ages. Two further cobbles from the Deseado 2 outwash yielded ages of 520 ka and 618 ka, the oldest of which agrees, within errors, with a modelled depth profile age of 600 ka (+70/-35) from the same outwash unit. The agreement between older ages from surface cobbles and the Deseado 2 depth profile is unsurprising given that modelling suggests surface erosion (<0.2 cm.ka^{-1}) and inheritance within

25   the outwash sediments ($<2.10^4$ atomg.g^{-1}) was relatively low (see Supplementary Information). There are a number of factors that can result in some age scatter within outwash surface cobbles, including surface deflation and up-freezing of clasts (Darvill et al. (2015); Hein et al. (2017)). Moreover, Hein et al. (2009,

2017) suggested that the oldest surface exposure ages from outwash in this region will most closely relate to deposition age. The D2-T12 sample is >200 ka younger than the other Deseado 2 cobbles, and it is likely that this cobble was either deposited at a much later time (perhaps during Moreno-stage glaciation, although the difference in altitude makes this unlikely) or was not in situ. The close agreement between other Deseado 2 ages supports the removal of D2-T12 as an outlier. Finally, a modelled depth profile through outwash relating to the Telken 5 moraine produced an age of 780 ka (+170/-80, 1σ confidence interval), with relatively low surface erosion (<0.1 cm ka-1) and inheritance (<6.10^4 atomg.g^{-1}). This age is within the lower range of 760-1016 ka known from radiometric ages (Singer et al., 2004). Sensitivity tests showed that modifications of the a priori values of erosion rates and inheritance lead to insignificant changes in the resulting age.

3.2   Evaluation of the U-Th chemical procedure with SEM images

For three samples taken randomly, we looked at SEM images after 50μm sieving and preparation (Figure 4) to assess the effects of our chemical and mechanical treatment. We were particularly interested in whether secondary phases could remain after processing, and if the primary silicates could have been altered by this treatment. The minerals observed are mainly quartz, feldspars and micas, corresponding to the lithology of the Andes in these latitudes. We list below the main observations :

– No trace of carbonate, organic matter or oxides were observed in samples that underwent the entire protocol. Prior to treatment, we only note the presence of oxides (Figure 4b). This does not, however, preclude the presence of carbonate or organic matter since a difference of mass before and after steps 2 and 5 of the protocol were observed. Therefore, the protocol seems efficient at eliminating carbonates, oxides, and organic matter.

– Samples were generally cleaner after preparation. This is because ≤ 4 μm fractions, containing mainly clays, were removed by Stokes settling. However, clays are still observed in the samples after preparation (see Figure 4b and c), mainly agglomerated around primary grains as clay pellets. In one sample, up to one third of the grains have clay pellets. These clays could have been precipitated directly at the surface of the grains during weathering or agglomerated subsequently. It is difficult to fully eliminate the clays and a potential bias could be introduced if too many clays remain in the sample. This po-

tentially limits the application of comminution ages to samples with very low amount of clays, since their complete removal is currently not possible.

– Most micas show surfaces having experienced weathering (Figure 4d). The shapes observed are typical of weathering both before and after the protocol. This shows that our silts samples have experienced weathering and that it could potentially have affected U-Th disequilibrium.

– Following the preparation protocol, two feldspar grains in one sample displayed evidence of corrosion (Figure 4e and 4f). While this damage could be associated with alteration of the primary silicates during leaching, these are the only two corroded grains visible in the samples we tested. Since the corrosion pits are smaller than 4μm, and all the grains are larger than 4μm in our samples, ubiquitous damage would be observable on other grains. As such, we assume that primary mineral corrosion during the protocol is minimal.

3.3 U-Th - f_α - age

U-Th results are shown on Figure 5 and Table 3. $(^{234}U/^{238}U)$ from moraines display little variation, ranging from 0.95 to 0.97, while glacial flour has a composition of 1.007, close to equilibrium. For the moraine samples, a general decrease of $(^{234}U/^{238}U)$ is observed with time, though with significant noise. $(^{230}Th/^{238}U)$ mostly vary between 0.94 and 0.97 with the youngest moraine sample (F1-U-M2, Fenix moraine) having a composition around 1. Similarly $(^{230}Th/^{234}U)$ mostly range from 0.99 and 1.01, with the youngest moraine around 1.03. Again, an overall decrease in $(^{230}Th/^{234}U)$ is observed with time. The glacial flour is close to equilibrium compositions $((^{230}Th/^{238}U)=1.02$ and $(^{230}Th/^{234}U)=1.01)$. Specific surface areas vary from 1.5 to 7 m^2/g, which is typical for this kind of samples, and the fractal dimensions range from 2.45 to 2.6. The recoil loss factors f_α calculated using equations 3 are between 0.005 and 0.025, with no observable trend with time.

Handley et al. (2013a) analyzed only a few samples with the gas adsorption technique to characterize the specific surface area and f_α. We analyzed every sample with this technique, highlighting the consistency of the noise in $(^{234}U/^{238}U)$ and the dispersion in f_α derived from specific surface area (Figure 5). The relationship between $(^{234}U/^{238}U)$, f_α and age is described by a surface in three dimensions. In other words, the noise observed in the $(^{234}U/^{238}U)$-age diagram, around the general decreasing pattern is in a large part

associated with the dispersion of f_α. This suggests that specific surface area data are consistent and reliable, or that, if a bias exist in these data, it is systematic. Such a systematic bias would arise from a rather random event due to the sample processing, so this latter explanation seems unreasonable. We conclude that the specific surface area determination based on the gas adsorption technique is valid to evaluate the recoil loss

5 factor in the U-Th comminution age theory.

We observe that (^{230}Th/^{234}U) is larger than (^{234}U/^{238}U) and (^{230}Th/^{238}U) has comparable compositions to (^{234}U/^{238}U). As mentioned in section 2.3.1, this observation is incompatible with a simple comminution age model (only α-recoil). An enrichment of ^{230}Th compared to ^{234}U could be the imprint of weathering on silts found in the moraines. Similarly, the incompatibilities of (^{234}U/^{238}U) and f_α in the framework of the

10 simple comminution age model suggest that weathering must be considered. In the comminution age theory as described by DePaolo et al. (2006), $1 - f_\alpha$ must always be lower than (^{234}U/^{238}U), and for a sample old enough to have reached steady state, (^{234}U/^{238}U)=$1 - f_\alpha$. This is not what we observe, similarly to Handley et al. (2013a). However, as described in section 2.3.1 such an observation can be explained if weathering is considered and $k_{234} \geq k_{238}$.

15 Given the large disequilibrium of the youngest samples in (^{234}U/^{238}U) and in (^{230}Th/^{234}U) (Table 3 and Figure 5), and the fact that the glacial flour (the most probable inital composition for the moraine silts) is close to equilibrium, we cannot ignore the pre-depositional history (i.e. before deposition in the moraines). Based on a starting value close to equilibrium, the disequilibrium values measured here cannot be reached in only 20, or even 200 ka. Since our estimations of the f_α seem consistent and reliable, this requires

20 consideration of a pre-depositional history involving weathering with a different intensity than during the post-deposition history.

3.4 Predeposition history and Monte Carlo analysis

We attempt to constrain the pre-depositional history using a Monte Carlo analysis. The results show an inverse relationship, with the greatest probability for $k_{238}^{pre}/k_{238}^{post}$ between 2 and 3 and a recycling time between

25 100 and 200 kyrs. The optimal values of k_{234}/k_{238} and k_{230}/k_{238} associated with this solution describe an anti-correlation with $1.2 \leq k_{234}/k_{238} \leq 2$ and $0.01 \leq k_{230}/k_{238} \leq 0.8$ (figure 6). These parameters are, however, poorly constrained by the inversion process.

Despite the numerous parameters to be constrained, the model converges for key results as shown above. We show in particular that, in the framework of the modified comminution age theory', incorporating weathering, described in section 2.3.1, we can say that the silts from the LBA moraines were likely eroded 100 to 200 kyrs before being deposited in the moraines and that, on average, they experienced around 2-3 times

5   more intense weathering during this interval than after deposition (Figure 6). The best fit, corresponding to a recycling time of 180 kyrs, a ratio $k_{238}^{pre}/k_{238}^{post} = 2.35$, $k_{234}/k_{238} = 1.4$, and $k_{230}/k_{238} = 0.6$, is shown on supplementary Figure 5.

4   Discussion

4.1   Glacial chronology and perspectives on the control of ice extent in the Patagonian Andes

10   The new [10]Be exposure ages in this study help clarify the timing of deposition of several of the LBA moraines. The oldest outwash cobbles are taken as closest to the age of deposition because depth profiles show that average nuclide inheritance is relatively low and outwash surfaces show evidence for deflation (exposing younger cobbles; Hein et al. (2011, 2017)). It is possible that even the oldest cobbles underestimate the age of deposition if they have also been exhumed, and we apply no erosion correction to our exposure

15   ages. As discussed in Hein et al. (2017), outwash surface cobbles imply that the Moreno moraines were deposited at ca. 260-270 ka, during Marine Isotope Stage 8.

Unlike the Moreno system, surface cobbles from the Deseado moraines appear to date from two different glacial cycles. Exposure ages from Deseado 1 outwash yield relatively tightly clustered ages of 430-470 ka, suggesting that the limit was deposited during MIS 12. The older of two published moraine boulder

20   exposure ages from the Deseado 1 moraine (erosion-corrected to 476 ka; Kaplan et al. (2005)) is consistent with the cobble ages in this study. In contrast, surface cobbles from Deseado 2 outwash yield ages of 520 ka and 618 ka (excluding the anomalously young D2-T12 age of 293 ka). The dating would be less conclusive without the accompanying depth profile age of 600 +70/-35 ka. Slight changes in scaling factors (see section 2.2.3) do not affect this finding. Taken together, the oldest surface cobble and depth profile suggest that

25   the Deseado 2 limit was deposited at ca. 600-620 ka. Within errors, the limit may relate to MIS 16. The scatter in ages is interesting given that luminescence dating yielded an even younger age of 123 ± 18 ka for the Deseado 2 limit (Smedley et al., 2016). This scatter may imply greater sediment reworking or a more

complex relationship between moraines and outwash in this sequence. The Telken 5 depth profile gave an age of 780 +170/-80 ka that is stratigraphically consistent within our chronological dataset, but less helpful in determining when the limit was deposited. The error range spans MIS 18-24 (and radiometric datings gave a lower age of 760 ka for the Telken serie), with larger probability around MIS 20, so it is possible that

5   the moraine was deposited during MIS 20. Since the entire Telken moraine system must be older than 760 ka (Singer et al., 2004), this implies that Telken 1 to 4 are also that age, and that the Telken moraines represent different glacial advances during the same glacial cycle.

In summary, there is a clear pattern in the timing of moraine deposition in which alternate glacial cycles are represented in our chronology: Telken 5 during MIS 20; Deseado 2 during MIS 16; Deseado 1 during MIS

10   12; and the Moreno moraines during MIS 8. Previous work has shown that the innermost Fenix moraines relate to the Last Glacial Maximum during MIS 2 (Kaplan et al. (2004); Douglass et al. (2006); Smedley et al. (2016)). We strongly caution that scatter in surface cobble ages and error ranges in depth profiles may complicate this pattern, particularly for the older limits. Moreover, we did not analyse the enigmatic Deseado 3 moraine and so cannot say whether this relates to the counterparts dated here or intervening glacial stages.

15   However, dating of the Moreno and Deseado 1 and 2 moraines does imply that the intervening glacial cycle is absent from the record.

The pattern in timing of moraine deposition around Lago Buenos Aires implies that there are a few glacial cycles that are either not recorded in this area, or have been erased or removed. Either the ice lobe did not advance during alternate glacial cycles, or advanced to similar or less extensive positions so that moraines

20   and outwash were then removed by the following advance. A similar pattern was observed by Hein et al. (2009, 2011) for the Lago Pueyrredon ice lobe, 100 km to the south, and so there could be a regional driver of alternate glacial advances. One possibility is that erosion over successive glacial cycles caused entrenchment of ice lobes within large basins on the eastern side of the Patagonian Ice Sheet (Kaplan et al., 2009). This erosion model has been linked to the pattern of nested limits seen across the former ice sheet (Kaplan et al.,

25   2009; Anderson et al., 2012) but may be more complex if only alternate cycles are represented in the moraine record. Alternatively, a purely climatic forcing could have caused alternate strong advances, although there is no simple relationship between available climate records and alternate glacial advances at Lago Buenos Aires. A complex erosion-climate feedback mechanism may determine when or how far glacial advances occurred in this region, but more detailed glacial models are required to further test such a model.

The chronology presented here suggests that moraines reworking has probably occured in the area, and/or that glacial erosion in the Andes may feedback into the glacial lobe advance, to produce this observed pattern of absent intervening glacial cycles. Regardless, this chronology allows us to broadly constrain deposition ages of moraines targeted for U-Th analysis, which may in turn inform sediment recycling times between preserved moraines.

4.2 Implications for sediment recycling, chemical weathering, climate and their interactions, in proglacial systems

Following the conclusions of Handley et al. (2013a), this residence time of 100-200 kyrs could be an artifact due to an addition of old dust. In our area, when a new moraine is being formed, the older sediments are on the east, whereas the dominant winds comes from the west. So it is unlikely that these winds could add older material to the one being deposited.

The long time estimated using the whole set of data and the Monte Carlo simulations, along with the absence of inheritance in the [10]Be data, suggest that the sediment was not exposed at the surface in the proglacial system before being deposited in its moraine. This implies that the sediment must have been buried, either in the proglacial lake, or within a sedimentary pile (moraine, till, channel, etc. at least a few meters below the surface) before final deposition.

The dated sediment was most probably eroded during glacial periods, as erosion rates are likely much larger than during interglacial. Likewise, deposition in an end moraine occurs during a glacial period. This means that the sediment deposited in the moraine may spend on average as long as 100-200 kyrs in the proglacial system (till, lakes sediments, etc.) before being deposited in the moraines. Hence the sediment eroded during a glacial period is, on average, deposited in the frontal moraine during the next glacial cycle. Using postglacial sediment budget and reservoir theory, Hoffmann & Hillebrand (2016) modelled the residence time of sediments in a periglacial system in the Canadian Rocky Mountains, and also found a time of 100 kyrs. This average residence time implies that a fraction of the sediment deposited in a moraine may have been produced during the same glacial cycle and with an other fraction being much older.

This time appears to be long. However, our measurements of cosmogenic exposure ages using [10]Be nuclide concentrations in outwash cobbles and profiles suggest that the preserved moraines represent every other glacial cycle, indicating an advance over the proglacial sediment of one or two previous advances.

Moreover, it has been shown that proglacial lakes occupying overdeepenings are filled following deglaciation (Eyles et al., 1991; Houbolt & Jonker, 1968). The lakes are filled with sediments during interglacial periods, and emptied during the subsequent glacial periods. These processes imply sediment erosion and deposition over a full glacial-interglacial cycle which is consistent with both ^{10}Be and U-Th disequilibrium data.

We also obtain weathering rate that is 2-3 times higher during the 100-200 kyrs of the predepositional phase than after deposition. Based on the argument above, these sediments are exposed to water in the proglacial system before deposition in the moraine. Authors such as Anderson (2005) have shown that proglacial environments favor weathering. Since weathering rate is a time dependent parameter (e.g. White & Brantley (2003)), this recycling time of 100-200 kyrs has a likely non-negligible impact on weathering fluxes.

Understanding how sediments are evacuated and transported to the oceans, and when they experience weathering would help to quantify the relationships between erosion and climate. In particular, if 100 to 200 kyrs are needed to escape the periglacial area, important lags could be observed between the erosion forcing, and the weathering and climate response. This suggests that measured weathering variations could have occured over the last glacial-interglacial cycles, or have been smoothed/damped because of a lag in the sediment transport. Estimating these lag times would help understand the relationships between erosion, climate, and marine biogeochemical cycles. Erosion rates can be determined using thermochronology or cosmogenic isotopes. Sedimentation rates in the ocean can be estimated as well using marine core dating methods. The link between erosion and sedimentation is poorly known (Sadler, 1981) especially because the transport times are poorly constrained. The transport time of 100 to 200 kyrs presented here suggests that the pathway between initial erosion and deposition is potentially complex. An effort to constrain these transport times appears to be potentially fruitful to reveal the actual link between erosion/sedimentation rates and climate.

4.3 Perspectives on comminution age method and its applications to characterize sediment transfer

Our data let us estimate only a mean recycling time for moraine sediment (the fine silty fraction). Here we have discussed it in terms of recycling of the previous glacial cycle moraine, but it could also be interpreted as a mixing of much older, deeper, reworked sediment with new freshly eroded sediment. In other words, we

do not quantify the amount of sediment escaping the proglacial system, or the amount of sediment which is deposited in the moraine rapidly after erosion. It would be beneficial to think about ages distributions, and not only mean ages. However, this necessitates being able to measure U-Th disequilibrium on single grains, which remains an analytical challenge (Bosia et al., submitted).

5   Quantifying or reducing the effects of weathering remains a major challenge. Pure primary minerals with no clays would minimise these secondary processes. To this end, working on pure zircons grains could be an option. This would require improved mineral separation methods for fractions smaller than 50 μm. One would also have to assume that comminution effectively occured on such a heavy mineral, and that there is no initial disequilibrium (a problem being that zircons are much enriched in U than there surrounding

10   minerals).

5 Conclusions

Our study is a first attept to quantify long term sediment transfer times in proglacial area. We take advantage of the particularly well preserved series of nested moraines of the Lago Buenos Aires in Patagonia. Our approach involves [10]Be exposure dating of these moraines combined with U-Th disequilibrium measure-

15   ment on the fine fraction of moraine sediment, within a 'modified' comminution theoretical framework, to characterize the pre-deposition and post-deposition histories of the sediments.

We show that weathering cannot be neglected when determining the comminution age. Measuring Th isotopes helps constrain the weathering process. Even with this complication, it remains possible to calculate comminution ages if the studied samples have well constrained deposition ages and have experienced the

20   same predepositional history. In this case, the weathering intensities and the predepositional history duration are the same for all the samples. We also show that specific surface area measurements based on the gas adsorption technique for estimation of the recoil loss factor is a reliable method, and should be applied to all samples. One caveat is that clay minerals may not be removed from the samples, especially clay pellets agglomerated at some mineral surfaces, which could be a strong limitation of the use of this method to

25   calculate transport times.

Our new chronology shows that some glacial cycles are either not preserved or not recorded in the LBA area, i.e. respectively the associated moraines may have been removed by following glacial advances or may

have been deposited farther upstream. Hein et al. (2011) found a similar pattern in Lago Pueyrredon area, suggesting that the mechanisms driving glacial advance may have a regional extent. Future work may reveal wether erosion feedbacks in the Andes could be responsible for this pattern.

The absence of moraine records for a few glacial cycles in the LBA area can be explained by our U-Th data showing that there has been reworking/recycling of the sediments. Using a Monte Carlo approach we estimate that the silts from the Lago Buenos Aires frontal moraines system have 100 kyr residence time in the proglacial system (transported in the lake sediments, remobilized from the previous moraines or stored in intermediate reservoirs), and experienced three times more intense weathering before deposition than in the moraine. Our data represent a step toward the effort of constraining the pathways and timescales over which sediments are transported from source (erosion in mountain belts) to sink (ocean sediments). Although considered as a daunting challenge by Sadler & Jerolmack (2015) and requiring additional development, this approach can contribute to our understanding of basin-scale sediment budgets and how erosion, weathering, and sedimentation evolve through time.

Code availability. TEXT

Data availability. TEXT

Code and data availability. TEXT

Author contributions.

Competing interests. The authors declare that they have no conflict of interest.

Disclaimer.

Acknowledgements. We thank the administration of the Laguna San Rafael National Park for delivering us the authorization of sampling in the glacier Los Exploradores area and especially Cristobal Fabres for his nice support and escort during the sampling.

References

Ackerer, J., Chabaux, F., Van der Woerd, J., Viville, D., Pelt, E., Kali, E., Lerouge, C., Ackerer, P., di Chiara Roupert, R., & Négrel, P. (2016). Regolith evolution on the millennial timescale from combined u–th–ra isotopes and in situ cosmogenic 10 be analysis in a weathering profile (strengbach catchment, france). *Earth and Planetary Science Letters*, *453*, 33–43.

Anderson, R., Dühnforth, M., Colgan, W., & Anderson, L. (2012). Far-flung moraines: Exploring the feedback of glacial erosion on the evolution of glacier length. *Geomorphology*, *179*, 269–285.

Anderson, S. (2005). Glaciers show direct linkage between erosion rate and chemical weathering fluxes. *Geomorphology*, *67*, 147–157.

Anderson, S., Drever, J., & Humphrey, N. (1997). Chemical weathering in glacial environments. *Geology*, *25*, 399–402.

Balco, G., Stone, J., Lifton, N., & Dunai, T. (2008). A complete and easily accessible means of calculating surface exposure ages or erosion rates from 10 be and 26 al measurements. *Quaternary geochronology*, *3*, 174–195.

Bendle, J., Thorndycraft, V., & Palmer, A. (2017). The glacial geomorphology of the lago buenos aires and lago pueyrredón ice lobes of central patagonia. *Journal of Maps*, *13*, 654–673.

von Blanckenburg, F., Bouchez, J., Ibarra, D., & Maher, K. (2015). Stable runoff and weathering fluxes into the oceans over quaternary climate cycles. *Nature Geoscience*, .

von Blanckenburg, F., Hewawasam, T., & Kubik, P. (2004). Cosmogenic nuclide evidence for low weathering and denudation in the wet, tropical highlands of sri lanka. *Journal of Geophysical Research: Earth Surface*, *109*.

Borchers, B., Marrero, S., Balco, G., Caffee, M., Goehring, B., Lifton, N., Nishiizumi, K., Phillips, F., Schaefer, J., & Stone, J. (2016). Geological calibration of spallation production rates in the cronus-earth project. *Quaternary Geochronology*, *31*, 188–198.

Bosia, C., Chabaux, F., Pelt, E., Cogez, A., Stille, P., Deloule, E., & France-Lanord, C. (submitted). U-series disequilibria in minerals from gandak river sediments (himalaya). *submitted to Chemical Geology*, .

Bosia, C., Chabaux, F., Pelt, E., France-Lanord, C., Morin, G., Lavé, J., & Stille, P. (2016). U–th–ra variations in himalayan river sediments (gandak river, india): Weathering fractionation and/or grain-size sorting? *Geochimica et Cosmochimica Acta*, *193*, 176–196.

Bourdon, B., Bureau, S., Andersen, M., Pili, E., & Hubert, A. (2009). Weathering rates from top to bottom in a carbonate environment. *Chemical Geology*, *258*, 275–287.

Chabaux, F., Blaes, E., Granet, M., di Chiara Roupert, R., & Stille, P. (2012). Determination of transfer time for sediments in alluvial plains using 238 u-234 u-230 th disequilibria: The case of the ganges river system. *Comptes Rendus Geoscience*, *344*, 688–703.

Chabaux, F., Blaes, E., Stille, P., di Chiara Roupert, R., Pelt, E., Dosseto, A., Ma, L., Buss, H., & Brantley, S. (2013). Regolith formation rate from u-series nuclides: implications from the study of a spheroidal weathering profile in the rio icacos watershed (puerto rico). *Geochimica et Cosmochimica Acta*, *100*, 73–95.

Chabaux, F., Bourdon, B., & Riotte, J. (2008). U-series geochemistry in weathering profiles, river waters and lakes. *Radioactivity in the Environment*, *13*, 49–104.

Chabaux, F., Riotte, J., & Dequincey, O. (2003). U-th-ra fractionation during weathering and river transport. *Reviews in Mineralogy and Geochemistry*, *52*, 533–576.

Chmeleff, J., von Blanckenburg, F., Kossert, K., & Jakob, D. (2010). Determination of the 10 be half-life by multicollector icp-ms and liquid scintillation counting. *Nuclear Instruments and Methods in Physics Research Section B: Beam Interactions with Materials and Atoms*, *268*, 192–199.

Christeleit, E., Brandon, M., & Shuster, D. (2017). Miocene development of alpine glacial relief in the patagonian andes, as revealed by low-temperature thermochronometry. *Earth and Planetary Science Letters*, *460*, 152–163.

Christl, M., Vockenhuber, C., Kubik, P., Wacker, L., Lachner, J., Alfimov, V., & Synal, H.-A. (2013). The eth zurich ams facilities: Performance parameters and reference materials. *Nuclear Instruments and Methods in Physics Research Section B: Beam Interactions with Materials and Atoms*, *294*, 29–38.

Cogez, A., Meynadier, L., Allègre, C., Limmois, D., Herman, F., & Gaillardet, J. (2015). Constraints on the role of tectonic and climate on erosion revealed by two time series analysis of marine cores around new zealand. *Earth and Planetary Science Letters*, *410*, 174–185.

Darvill, C. M., Bentley, M. J., Stokes, C. R., Hein, A. S., & Rodés, Á. (2015). Extensive mis 3 glaciation in southernmost patagonia revealed by cosmogenic nuclide dating of outwash sediments. *Earth and Planetary Science Letters*, *429*, 157–169.

DePaolo, D., Maher, K., Christensen, J., & McManus, J. (2006). Sediment transport time measured with u-series isotopes: results from odp north atlantic drift site 984. *Earth and Planetary Science Letters*, *248*, 394–410.

DePaolo, D. J., Lee, V. E., Christensen, J. N., & Maher, K. (2012). Uranium comminution ages: Sediment transport and deposition time scales. *Comptes Rendus Geoscience*, *344*, 678–687.

Dequincey, O., Chabaux, F., Clauer, N., Sigmarsson, O., Liewig, N., & Leprun, J.-C. (2002). Chemical mobilizations in laterites: evidence from trace elements and 238 u-234 u-230 th disequilibria. *Geochimica et Cosmochimica Acta*, *66*, 1197–1210.

Dosseto, A., Bourdon, B., & Turner, S. P. (2008). Uranium-series isotopes in river materials: insights into the timescales of erosion and sediment transport. *Earth and Planetary Science Letters*, *265*, 1–17.

Dosseto, A., Buss, H., & Chabaux, F. (2014). Age and weathering rate of sediments in small catchments: The role of hillslope erosion. *Geochimica et Cosmochimica Acta*, *132*, 238–258.

Dosseto, A., Buss, H., & Suresh, P. (2012). Rapid regolith formation over volcanic bedrock and implications for landscape evolution. *Earth and Planetary Science Letters*, *337*, 47–55.

Dosseto, A., Hesse, P., Maher, K., Fryirs, K., & Turner, S. (2010). Climatic and vegetation control on sediment dynamics during the last glacial cycle. *Geology*, *38*, 395–398.

Dosseto, A., & Schaller, M. (2016). The erosion response to quaternary climate change quantified using uranium isotopes and in situ-produced cosmogenic nuclides. *Earth-Science Reviews*, *155*, 60–81.

Douglass, D., Singer, B., Kaplan, M., Mickelson, D., & Caffee, M. (2006). Cosmogenic nuclide surface exposure dating of boulders on last-glacial and late-glacial moraines, lago buenos aires, argentina: interpretive strategies and paleoclimate implications. *Quaternary Geochronology*, *1*, 43–58.

Ebelmen, J. (). Sur les produits de la décomposition des espèces minérales de la famille des silicates. *Annales des Mines*, .

Eyles, N., Mullins, H., & Hine, A. (1991). The seismic stratigraphy of okanagan lake, british columbia; a record of rapid deglaciation in a deep 'fiord-lake' basin. *Sedimentary Geology*, *73*, 13–41.

Foster, G., & Vance, D. (2006). Negligible glacial–interglacial variation in continental chemical weathering rates. *Nature*, *444*, 918–921.

Gontier, A. (2014). *Quantification de l'altération dans les sols par les déséquilibres radioactifs: approche sur sol total et phases minérales séparées*. Ph.D. thesis Strasbourg.

Granet, M., Chabaux, F., Stille, P., Dosseto, A., France-Lanord, C., & Blaes, E. (2010). U-series disequilibria in suspended river sediments and implication for sediment transfer time in alluvial plains: the case of the himalayan rivers. *Geochimica et Cosmochimica Acta*, *74*, 2851–2865.

Granet, M., Chabaux, F., Stille, P., France-Lanord, C., & Pelt, E. (2007). Time-scales of sedimentary transfer and weathering processes from u-series nuclides: clues from the himalayan rivers. *Earth and Planetary Science Letters*, *261*, 389–406.

Hallet, B., Hunter, L., & Bogen, J. (1996). Rates of erosion and sediment evacuation by glaciers: a review of field data and their implications. *Global and Planetary Change*, *12*, 213–235.

Handley, H., Turner, S., Afonso, J., Dosseto, A., & Cohen, T. (2013a). Sediment residence times constrained by uranium-series isotopes: a critical appraisal of the comminution approach. *Geochimica et Cosmochimica Acta*, *103*, 245–262.

Handley, H., Turner, S., Dosseto, A., Haberlah, D., & Afonso, J. (2013b). Considerations for u-series dating of sediments: Insights from the flinders ranges, south australia. *Chemical Geology*, *340*, 40–48.

Hashimoto, T., Aoyagi, Y., Kudo, H., & Sotobayashi, T. (1985). Range calculation of alpha-recoil atoms in some minerals using lss-theory. *Journal of radioanalytical and nuclear chemistry*, *90*, 415–438.

Hein, A., Cogez, A., Darvill, C., Mendelova, M. R., M.and Kaplan, Herman, F., Dunai, T., Norton, K., Xu, S., Christl, M. et al. (2017). Regional mid-pleistocene glaciation in central patagonia. *Quaternary Science Reviews*, *164*, 77–94.

Hein, A., Dunai, T., Hulton, N., & Xu, S. (2011). Exposure dating outwash gravels to determine the age of the greatest patagonian glaciations. *Geology*, *39*, 103–106.

Hein, A., Hulton, N., Dunai, T., Schnabel, C., Kaplan, M., Naylor, M., & Xu, S. (2009). Middle pleistocene glaciation in patagonia dated by cosmogenic-nuclide measurements on outwash gravels. *Earth and Planetary Science Letters*, *286*, 184–197.

Hidy, A., Gosse, J., Pederson, J., Mattern, J., & Finkel, R. (2010). A geologically constrained monte carlo approach to modeling exposure ages from profiles of cosmogenic nuclides: An example from lees ferry, arizona. *Geochemistry, Geophysics, Geosystems*, *11*.

Hoffmann, T., & Hillebrand, G. (2016). Sediment residence time and connectivity in non-equilibrium and transient geomorphic systems. In *EGU General Assembly Conference Abstracts* (p. 17509). volume 18 of *EGU General Assembly Conference Abstracts*.

Houbolt, J., & Jonker, J. (1968). Recent sediments in the eastern part of the lake of geneva (lac leman). *Geologie en Mijnbouw*, *47*, 131–148.

Kaplan, M., Ackert, R., Singer, B., Douglass, D., & Kurz, M. (2004). Cosmogenic nuclide chronology of millennial-scale glacial advances during o-isotope stage 2 in patagonia. *Geological Society of America Bulletin*, *116*, 308–321.

Kaplan, M., Douglass, D., Singer, B., Ackert, R., & Caffee, M. (2005). Cosmogenic nuclide chronology of pre-last glacial maximum moraines at lago buenos aires, 46 s, argentina. *Quaternary Research*, *63*, 301–315.

Kaplan, M., Hein, A., Hubbard, A., & Lax, S. (2009). Can glacial erosion limit the extent of glaciation? *Geomorphology*, *103*, 172–179.

Kaplan, M., Strelin, J., Schaefer, J., Denton, G., Finkel, R., Schwartz, A., R.and Putnam, Vandergoes, M., Goehring, B., & Travis, S. (2011). In-situ cosmogenic 10 be production rate at lago argentino, patagonia: implications for late-glacial climate chronology. *Earth and Planetary Science Letters*, *309*, 21–32.

Keech, A., West, A., Pett-Ridge, J., & Henderson, G. (2013). Evaluating u-series tools for weathering rate and duration on a soil sequence of known ages. *Earth and Planetary Science Letters*, *374*, 24–35.

Koppes, M., & Montgomery, D. (2009). The relative efficacy of fluvial and glacial erosion over modern to orogenic timescales. *Nature Geoscience*, *2*, 644–647.

Korschinek, G., Bergmaier, A., Faestermann, T., Gerstmann, U., Knie, K., Rugel, G., Wallner, A., Dillmann, I., Dollinger, G., Von Gostomski, C. et al. (2010). A new value for the half-life of 10 be by heavy-ion elastic recoil detection and liquid scintillation counting. *Nuclear Instruments and Methods in Physics Research Section B: Beam Interactions with Materials and Atoms*, *268*, 187–191.

Kubik, P. W., & Christl, M. (2010). 10 be and 26 al measurements at the zurich 6mv tandem ams facility. *Nuclear Instruments and Methods in Physics Research Section B: Beam Interactions with Materials and Atoms*, *268*, 880–883.

Lal, D. (1991). Cosmic ray labeling of erosion surfaces: in situ nuclide production rates and erosion models. *Earth and Planetary Science Letters*, *104*, 424–439.

Lee, V., DePaolo, D., & Christensen, J. (2010). Uranium-series comminution ages of continental sediments: Case study of a pleistocene alluvial fan. *Earth and Planetary Science Letters*, *296*, 244–254.

Lee, V. E. (2009). *Radiogenic isotope geochemistry and the evolution of the Earth's surface and interior*. Ph.D. thesis.

Leleyter, L., & Probst, J. (1999). A new sequential extraction procedure for the speciation of particulate trace elements in river sediments. *International Journal of Environmental Analytical Chemistry*, *73*, 109–128.

Lupker, M., France-Lanord, C., Galy, V., Lavé, J., & Kudrass, H. (2013). Increasing chemical weathering in the himalayan system since the last glacial maximum. *Earth and Planetary Science Letters*, *365*, 243–252.

Ma, L., Chabaux, F., Pelt, E., Granet, M., Sak, P. B., Gaillardet, J., Lebedeva, M., & Brantley, S. L. (2012). The effect of curvature on weathering rind formation: Evidence from uranium-series isotopes in basaltic andesite weathering clasts in guadeloupe. *Geochimica et Cosmochimica Acta*, *80*, 92–107.

Ma, L., Chabaux, F., West, N., Kirby, E., Jin, L., & Brantley, S. (2013). Regolith production and transport in the susquehanna shale hills critical zone observatory, part 1: Insights from u-series isotopes. *Journal of Geophysical Research: Earth Surface*, *118*, 722–740.

Maher, K., DePaolo, D., & Christensen, J. (2006). U–sr isotopic speedometer: fluid flow and chemical weathering rates in aquifers. *Geochimica et Cosmochimica Acta*, *70*, 4417–4435.

Mercer, J., & Sutter, J. F. (1982). Late miocene—earliest pliocene glaciation in southern argentina: implications for global ice-sheet history. *Palaeogeography, Palaeoclimatology, Palaeoecology*, *38*, 185–206.

Müller, A., Christl, M., Lachner, J., Suter, M., & Synal, H.-A. (2010). Competitive 10 be measurements below 1mev with the upgraded eth–tandy ams facility. *Nuclear Instruments and Methods in Physics Research Section B: Beam Interactions with Materials and Atoms*, *268*, 2801–2807.

Neymark, L. (2011). Potential effects of alpha-recoil on uranium-series dating of calcrete. *Chemical Geology*, *282*, 98–112.

Nishiizumi, K., Winterer, E., Kohl, C., Klein, J., Middleton, R., Lal, D., & Arnold, J. (1989). Cosmic ray production rates of 10be and 26al in quartz from glacially polished rocks. *Journal of Geophysical Research: Solid Earth*, *94*, 17907–17915.

Norton, K., von Blanckenburg, F., Schlunegger, F., Schwab, M., & Kubik, P. (2008). Cosmogenic nuclide-based investigation of spatial erosion and hillslope channel coupling in the transient foreland of the swiss alps. *Geomorphology*, *95*, 474–486.

Pelt, E., Chabaux, F., Innocent, C., Navarre-Sitchler, A., Sak, P. B., & Brantley, S. (2008). Uranium–thorium chronometry of weathering rinds: rock alteration rate and paleo-isotopic record of weathering fluids. *Earth and Planetary Science Letters*, *276*, 98–105.

Pelt, E., Chabaux, F., Stille, P., Innocent, C., Ghaleb, B., Gérard, M., & Guntzer, F. (2013). Atmospheric dust contribution to the budget of u-series nuclides in soils from the mount cameroon volcano. *Chemical Geology*, *341*, 147–157.

Sadler, P., & Jerolmack, D. (2015). Scaling laws for aggradation, denudation and progradation rates: the case for time-scale invariance at sediment sources and sinks. *Geological Society, London, Special Publications*, *404*, 69–88.

Sadler, P. M. (1981). Sediment accumulation rates and the completeness of stratigraphic sections. *The Journal of Geology*, (pp. 569–584).

Semkow, T. (1991). Fractal model of radon emanation from solids. *Physical review letters*, *66*, 3012.

Sims, K. W., Gill, J., Dosseto, A., Hoffmann, D. L., Lundstrom, C., Williams, R. W., Ball, L., Tollstrup, D., Turner, S., Prytulak, J. et al. (2008). An inter-laboratory assessment of the thorium isotopic composition of synthetic and rock reference materials. *Geostandards and Geoanalytical Research*, *32*, 65–91.

Singer, B., Ackert, R., & Guillou, H. (2004). 40ar/39ar and k-ar chronology of pleistocene glaciations in patagonia. *Geological Society of America Bulletin*, *116*, 434–450.

Smedley, R., Glasser, N., & Duller, G. (2016). Luminescence dating of glacial advances at lago buenos aires (46° s), patagonia. *Quaternary Science Reviews*, *134*, 59–73.

Stone, J. (1998). A rapid fusion method for separation of beryllium-10 from soils and silicates. *Geochimica et Cosmochimica Acta*, *62*, 555–561.

Stone, J. O. (2000). Air pressure and cosmogenic isotope production. *Journal of Geophysical Research: Solid Earth*, *105*, 23753–23759.

Tessier, A., Campbell, P., & Bisson, M. (1979). Sequential extraction procedure for the speciation of particulate trace metals. *Analytical chemistry*, *51*, 844–851.

Vance, D., Teagle, D., & Foster, G. (2009). Variable quaternary chemical weathering fluxes and imbalances in marine geochemical budgets. *Nature*, *458*, 493–496.

Walker, J. C., Hays, P., & Kasting, J. F. (1981). A negative feedback mechanism for the long-term stabilization of earth's surface temperature. *Journal of Geophysical Research: Oceans*, *86*, 9776–9782.

White, A., & Brantley, S. (2003). The effect of time on the weathering of silicate minerals: why do weathering rates differ in the laboratory and field? *Chemical Geology*, *202*, 479–506.
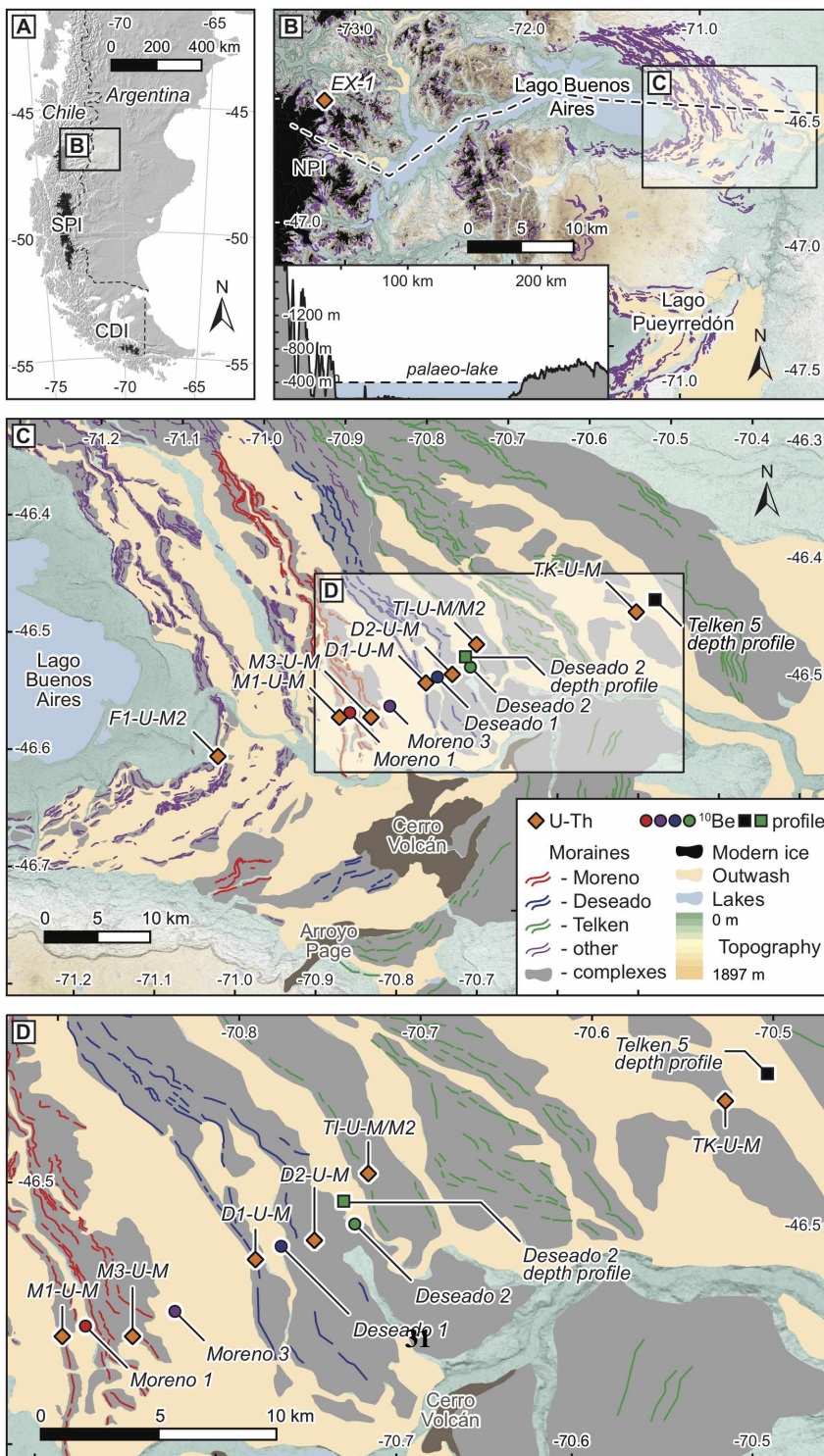
Figure 1. Map of the study area, adapted from Bendle et al. (2017). [A] Southern South America showing the location of Lago Buenos Aires. The three main contemporary ice masses in Patagonia are also shown: The Northern (NPI) and Southern Patagonian Icefields (SPI) and the Cordillera Darwin Icefield (CDI). [B] Inset shows a west-east transect through the study area, from the Patagonian Andes to the frontal moraine systems of the proglacial lake (adapted from Kaplan et al. (2009)); sample locations as per [a]. [C] and [D] The series of frontal moraines sampled in this study. Silt samples are shown by red circles and cobbles and profiles for cosmogenic analysis are shown in blue; the glacial flour sample at the mouth of Los Exploradores Glacier is shown; and the extent of the present day ice field is shown in black. Successive glaciations have formed the large over-deepening in which the proglacial lake has formed.
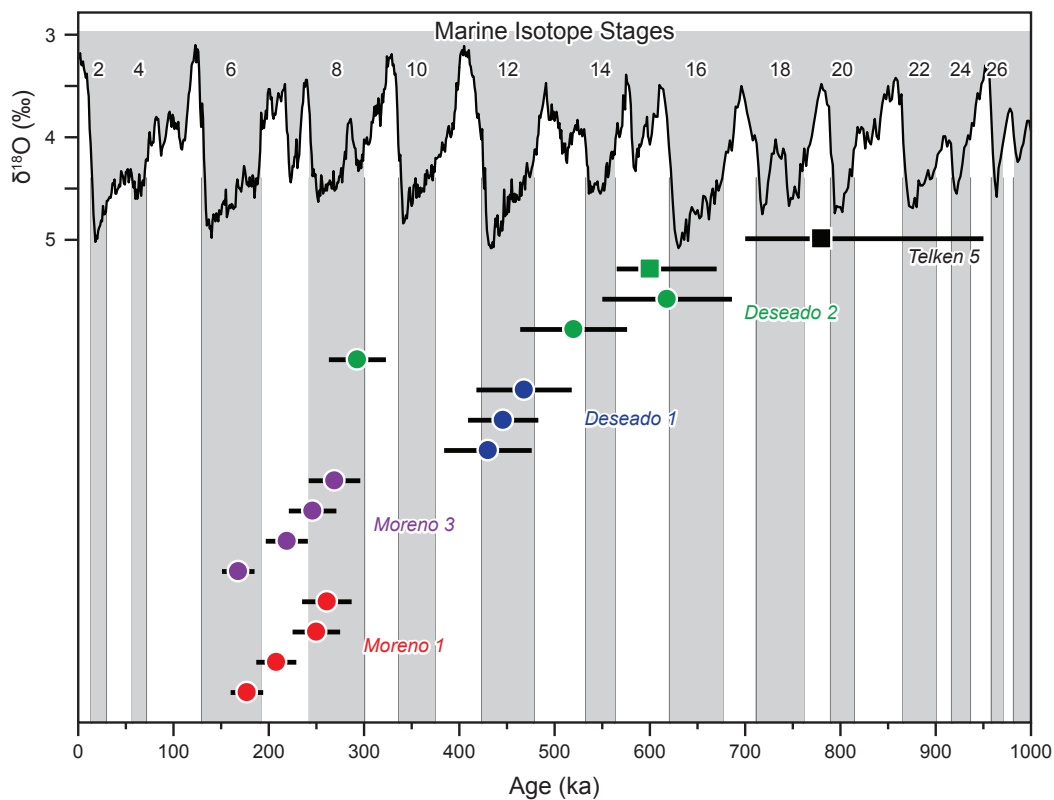
Figure 2. [10]Be exposure ages from outwash surface cobbles (circles) and modeled depth profiles (squares) for five of the Lago Buenos Aires moraines. Depth profile uncertainties are 1σ. Symbols and colors are the same as in figure 5. The δ^{18}O benthic stack record from Lisiecki Raymo (2005) is also plotted, and grey shading shows glacial stages.
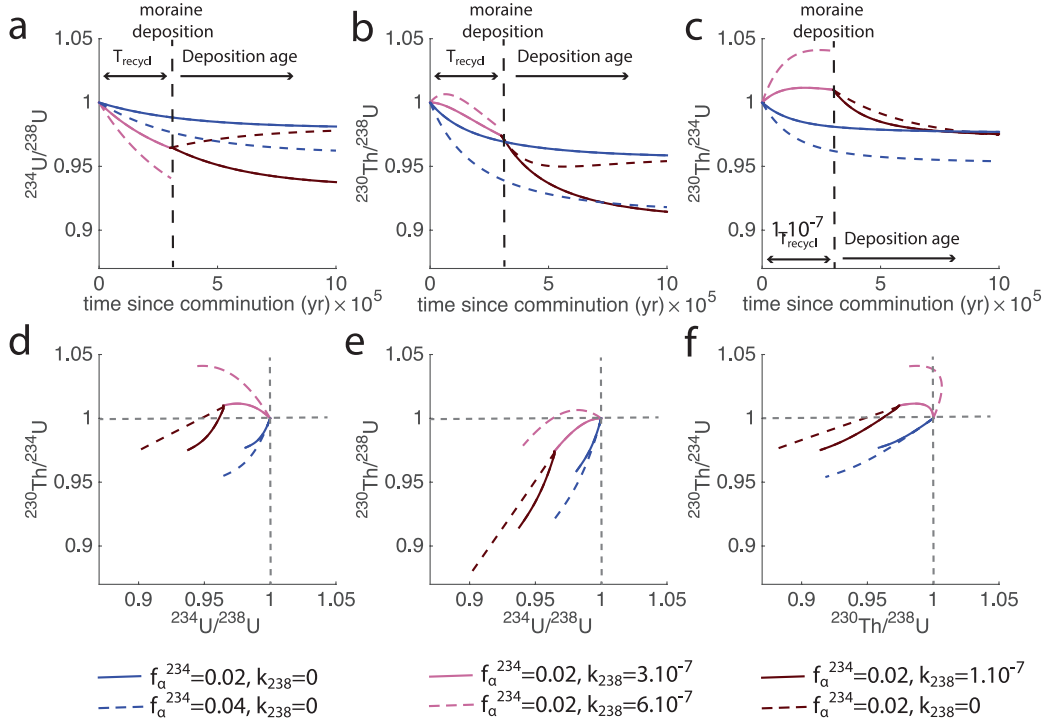
Figure 3. Solutions to the equations 2.3.1 that we use as the theoretical framework to analyze our data, for different values of f_α and k_{238} (We consider k_{234}/k_{238}=1.4 and k_{230}/k_{238}=0.5). (upper panels: a, b and c) the time evolution of $^{234}U/^{238}U$ (a), $^{230}Th/^{238}U$ (b) and $^{230}Th/^{234}U$ (c) activity ratios. The vertical dashed line represent an event through which the weathering intensity vary: this corresponds in our case to the time of sediment remobilization. Our ^{10}Be exposure ages give the time elapsed since this event (materialized by this dashed vertical line) whereas the U-Th data give the dureation of the first phase between comminution and remobilization, i.e. between Y axis and this dashed vetical line. (lower panels: d, e and f) the co-evolution of these ratios presented above. In order to make sense of the complexity of the different possible patterns in the framework of the comminution model incorporating weathering (see section 2.3.1. Different cases are plotted, corresponding to different f_α values, and different weathering intensities (see legend). Observing these figures helps to understand the range of variations of the different activity ratios, and the effect of each parameter (α-recoil and weathering) on these ratios, before and after remobilization of sediments.
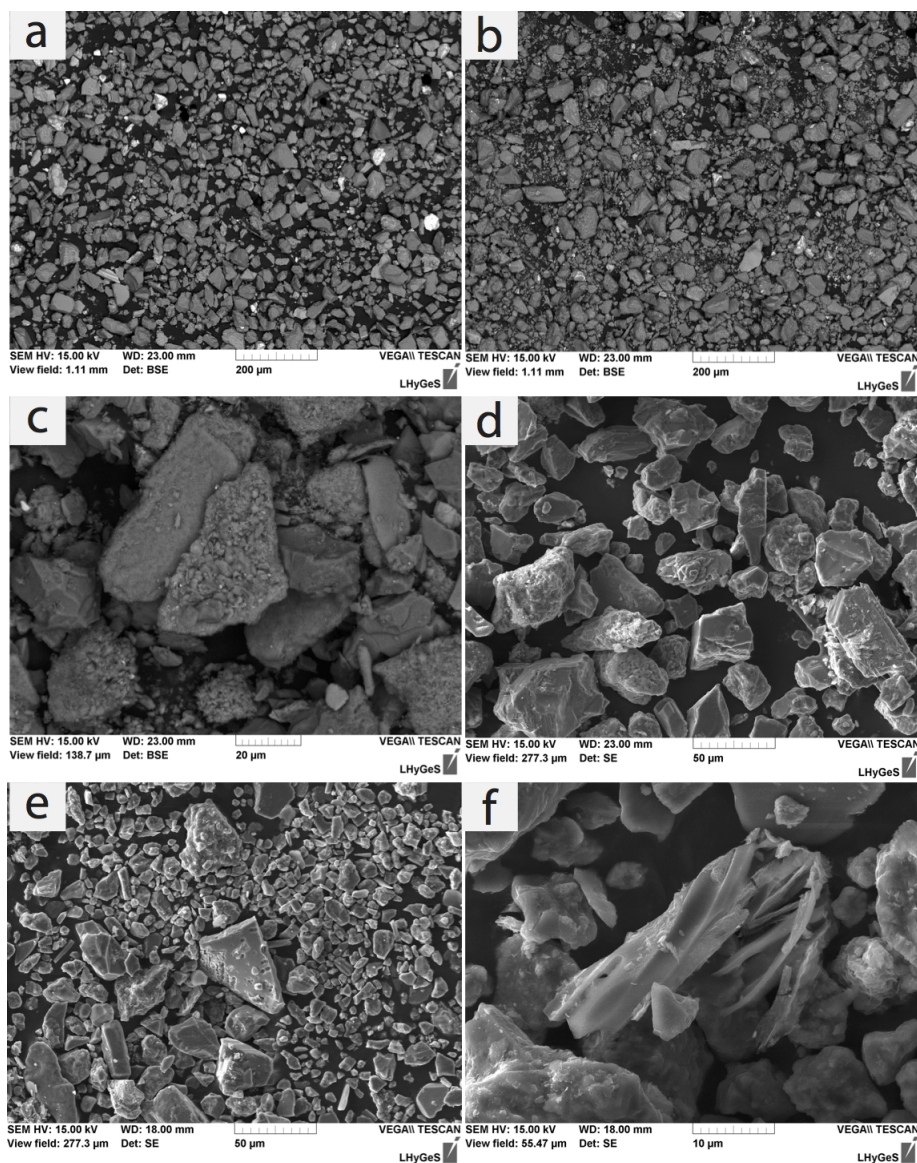
Figure 4. Scanning Electron Microscopy (SEM) images of selected samples. [a] Overview of a sample after the preparation process described in section 2.3.2. Grains vary in size and shape between 4 and 50μm and angular to subangular. White grains are heavy minerals such as zircon or oxides. [b] The same sample before 50μm sieving. The only notable difference is the presence of clays. [c] Zoomed image of a mineral grain covered in clays pellets that were not removed by the preparation process. [d] Mica grains with cauliflower faces, characteristic of weathering. [e] and [f] Feldspar grains with corroded surfaces. It is unclear whether these corrosion features result from geological processes or the sampling procedure, but they were only observed twice.
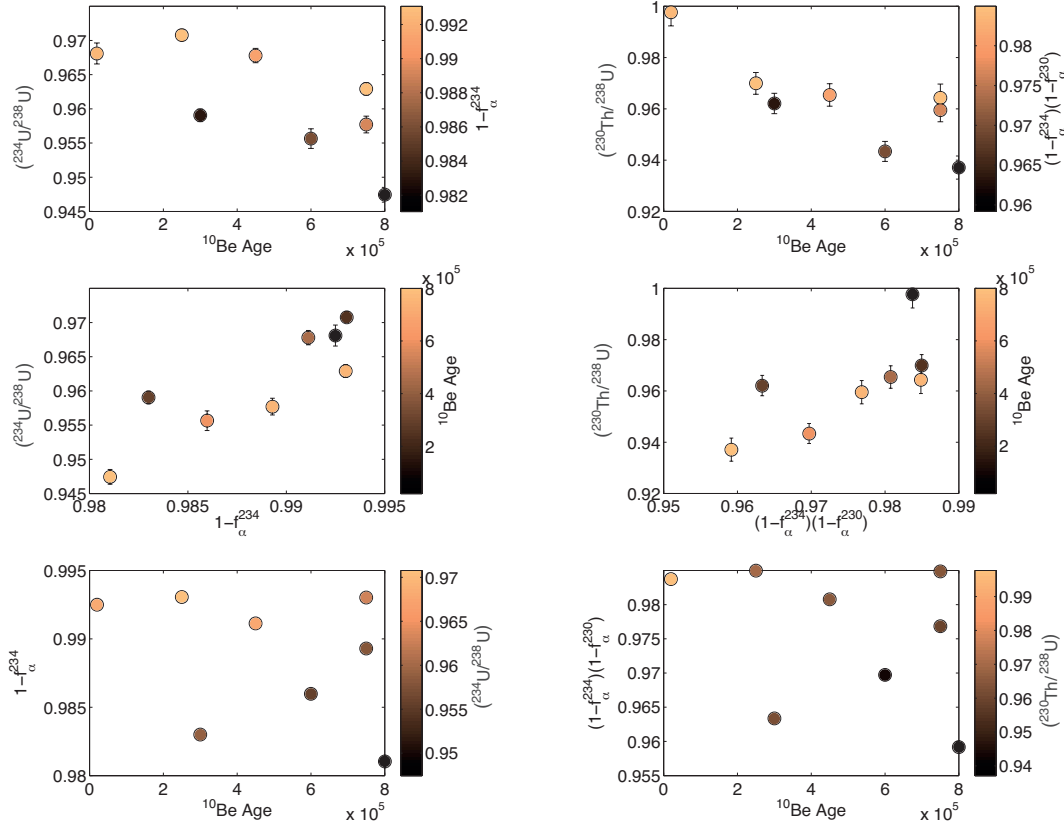
Figure 5. 2D cross plots of ^{234}U/^{238}U and ^{230}Th/^{238}U activity ratios; associated recoil loss factors $(1 - f_\alpha^{234})$ and $(1 - f_\alpha^{234}) \times (1 - f_\alpha^{230})$); and ^{10}Be exposure ages. Symbol colours represent the third parameter in each plot. Sorting observed in the symbol colours helps to explain the noise associated with the other two parameters. In particular, the scatter in the decrease of the activity ratios over time can be largely explained by the variability in the recoil loss factor (top left plot). The plots also let us assume that the variability in the weathering coefficients could be low, otherwise a residual dispersion would be observed. In all cases, error bars are smaller than the size of the dots.
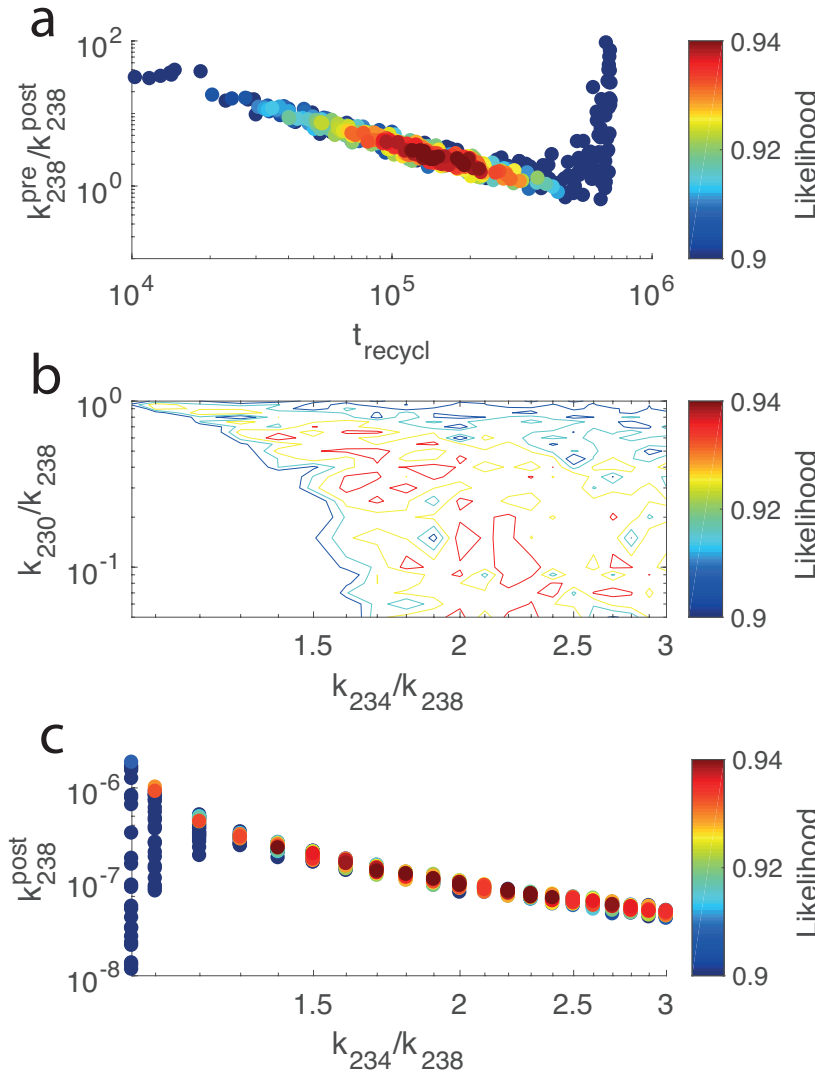
Figure 6. Results of Monte Carlo simulations for the U-Th data. The same Monte Carlo simulations were conducted for different fixed values of k_{234}/k_{238} and k_{230}/k_{238} (see section 2.3.5). For each simulation we estimated the optimal solution for k_{238}^{pre}, k_{238}^{post} and recycling time (pre-deposition duration, after comminution), i.e. the solution with the lowest misfit between measured and calculated activity ratio data. We used this misfit to calculate a likelihood between 0 and 1 (see equation 2.3.5), shown by the colourmap (red is lowest misfit, blue is higher misfit, stretched to fit our results). The larger the likelihood, the closer to the data the solution is, so the more likely the set of parameters values is. [a] The ratio $k_{238}^{pre}/k_{238}^{post}$ as a function of the recycling time. Each dot is one solution to the Monte Carlo. The optimal solution (red dots) is for three times stronger weathering before deposition and a recycling time of 100 ka. [b] Relative weathering intensities of ^{234}U, ^{238}U and ^{230}Th. The relative weathering intensities are poorly costrained, but a relationship can be extracted between their ratios : the larger k_{234}/k_{238}, the smaller k_{230}/k_{238} must be. [c] A relation between k_{238}^{post} and k_{234}/k_{238} can be extracted, even if both parameters are poorly constrained. So the estimation of sediment transfer times using U-Th disequilibria series could be improved with better constraints on the relative mobility ^{234}U, ^{238}U.

Table 1. Cosmogenic [10]Be nuclide data for outwash surface cobbles and depth profile samples. Moreno 1 and 3 data are already published in Hein et al. (2017).

Sample ID	Latitude (DD)	Longitude (DD)	Elev. (m asl)	Depth (cm)	Shielding correction	Thickness (cm)	^{10}Be/^{9}Be ($\times 10^{-12}$)	Sample weight (g)	^{9}Be added by carrier (10^{-4} g)	^{10}Be ± 1σ (10^5 at.g^{-1})
Moreno 1 outwash surface cobbles										
M1-T5	-46.5544	-70.8758	496	-	1	7	2.097 ±0.040	39.5464	3.046	10.75 ± 0.21
M1-T9	-46.5544	-70.8758	496	-	1	6.5	3.438 ±0.062	51.9881	2.867	12.64 ± 0.23
M1-T12	-46.5544	-70.8758	496	-	1	7	3.912 ±0.070	48.1040	2.875	15.59 ± 0.28
M1-T13	-46.5544	-70.8758	496	-	1	6	4.513 ±0.081	57.1220	2.864	15.09 ± 0.27
Moreno 3 outwash surface cobbles										
M3-T6	-46.547	-70.8268	482	-	1	7	1.939 ±0.058	38.8251	3.053	10.14 ± 0.31
M3-T11	-46.547	-70.8268	482	-	1	7	3.282 ±0.059	45.9404	3.052	14.53 ± 0.26
M3-T14	-46.547	-70.8268	482	-	1	4	4.299 ±0.116	61.5663	2.869	13.36 ± 0.36
M3-T16	-46.547	-70.8268	482	-	1	5	4.965 ±0.089	58.8835	2.857	16.07 ± 0.29
Deseado 1 outwash surface cobbles										
D1-T1	-46.5219	-70.7732	522	-	1	4	1.667 ±0.034	12.3329	2.866	25.75 ± 0.54
D1-T3	-46.5219	-70.7732	522	-	1	7	2.190 ±0.042	15.3978	2.863	27.10 ± 0.53
D1-T12	-46.5219	-70.7732	522	-	1	6.5	4.182 ±0.075	30.7913	2.882	26.11 ± 0.47
Deseado 2 outwash surface cobbles										
D2-T5	-46.5140	-70.7364	535	-	1	3	2.609 ±0.047	16.0937	2.879	31.09 ± 0.57
D2-T6	-46.5140	-70.7364	535	-	1	3	4.787 ±0.086	25.3782	2.874	36.16 ± 0.65
D2-T12	-46.5140	-70.7364	535	-	1	3.5	2.364 ±0.042	24.5217	2.882	18.50 ± 0.34
Deseado 2 outwash depth profile										
D2-50	-46.5015	-70.7368	544	50	1	4	2.889 ±0.052	37.9697	3.005	15.23 ± 0.28
D2-60	-46.5015	-70.7368	544	60	1	4	2.189 ±0.045	37.0362	3.044	11.97 ± 0.25
D2-70	-46.5015	-70.7368	544	70	1	4	1.905 ±0.037	37.1552	3.037	10.36 ± 0.21
D2-130	-46.5015	-70.7368	544	130	1	4	0.858 ±0.032	37.1738	3.050	4.65 ± 0.18
D2-230	-46.5015	-70.7368	544	230	1	4	0.307 ±0.013	43.5459	3.056	1.40 ± 0.07
Telken 5 outwash depth profile										
TK-50	-46.4439	-70.5069	552	50	1	4	2.402 ±0.053	27.4445	2.856	16.65 ± 0.37
TK-60	-46.4439	-70.5069	552	60	1	4	2.826 ±0.050	36.0118	3.045	15.92 ± 0.29
TK-70	-46.4439	-70.5069	552	70	1	4	2.516 ±0.049	35.8816	3.042	14.20 ± 0.28
TK-130	-46.4439	-70.5069	552	130	1	4	0.903 ±0.052	35.4972	3.048	5.13 ± 0.30
TK-240	-46.4439	-70.5069	552	240	1	4	0.417 ±0.024	42.5856	3.039	1.94 ± 0.12

Table 2. Modeled exposure ages for outwash surface cobbles and depth profile samples (see main text and Supplementary Information for details of profile modeling). Moreno 1 and 3 ages have been already publised in Hein et al. (2017).

Sample ID	Age (ka)	External error (ka)	Profile age (ka)	Upper error (ka)	Lower error (ka)
Moreno 1 outwash surface cobbles					
M1-T5	177	17			
M1-T9	208	21			
M1-T12	**261**	**26**			
M1-T13	250	25			
Moreno 3 outwash surface cobbles					
M3-T6	168	17			
M3-T11	246	25			
M3-T14	219	22			
M3-T16	**269**	**27**			
Deseado 1 outwash surface cobbles					
D1-T1	430	46			
D1-T3	**468**	**50**			
D1-T12	446	47			
Deseado 2 outwash surface cobbles					
D2-T5	520	56			
D2-T6	**618**	**68**			
D2-T12	*293*	*30*			
Deseado 2 outwash depth profile					
			600	70	35
Telken 5 outwash depth profile					
			780	170	80

Table 3. U-Th concentrations, activity ratios and BET data (specific surface areas and fractal dimensions, and calculated recoil loss factors). Duplicates are also shown, two for the whole process (including sieving, leachings, HF digestion, chromatography), and one for HF digestion and chromatography. The samples are sorted by deposition age (F1=Fenix, M1=Moreno 1, M3=Moreno3, D1=Deseado 1, D2 = Deseado 2, TI=Telken 1, TK=Telken 5).

sample	moraine	Latitude	Longitude	[U] (ppm)	2SE	[Th] (ppm)	2SE	Specific surface area (m2.g-1)	Fractal dimension	f_α^{234}
EX-1	glacial flour	-46.5026	-73.1642	4.186	0.010	22.70	0.06	1.051	2.49	0.0047
F1-U-M2	Fenix 1	-46.5974	-71.0359	1.680	0.002	6.36	0.01	1.831	2.52	0.0075
M1-U-M	Moreno 1	-46.5587	-70.8883	1.855	0.003	7.63	0.01	1.392	2.46	0.0069
M3-U-M	Moreno 3	-46.5574	-70.8494	2.148	0.003	8.67	0.02	4.719	2.56	0.0170
D1-U-M	Deseado 1	-46.5255	-70.7837	1.928	0.004	8.00	0.02	2.238	2.53	0.0089
D2-U-M	Deseado 2	-46.5170	-70.7518	1.503	0.002	5.94	0.01	3.535	2.53	0.0140
TI-U-M	Telken 1	-46.4904	-70.7240	1.633	0.003	6.56	0.01	2.081	2.45	0.0107
TK-U-M	Telken 5	-46.4552	-70.5292	1.593	0.003	6.96	0.02	5.435	2.57	0.0190
Duplicates			*Observation*							
M3-U-M 2	duplicate of the whole process			2.067	0.004	9.38	0.02	7.034	2.59	0.022
M3-U-M 2 bis	duplicate from the HF digestion step			1.990	0.003	8.52	0.02			
TI-U-M 2	duplicate of the whole process			1.776	0.003	6.92	0.01	1.818	2.54	0.0070

sample	moraine	(^{238}U/^{232}Th)	2SE	(^{234}U/^{238}U)	2SE	(^{230}Th/^{238}U)	2SE	(^{230}Th/^{234}U)	2SE
EX-1	glacial flour	0.561	0.002	1.007	0.001	1.022	0.005	1.015	0.005
F1-U-M2	Fenix 1	0.803	0.002	0.968	0.001	0.998	0.005	1.031	0.006
M1-U-M	Moreno 1	0.739	0.001	0.971	0.001	0.970	0.004	0.999	0.004
M3-U-M	Moreno 3	0.753	0.002	0.959	0.001	0.962	0.004	1.003	0.004
D1-U-M	Deseado 1	0.733	0.002	0.968	0.001	0.965	0.004	0.998	0.005
D2-U-M	Deseado 2	0.769	0.001	0.956	0.001	0.943	0.004	0.987	0.004
TI-U-M	Telken 1	0.757	0.002	0.958	0.001	0.960	0.005	1.002	0.005
TK-U-M	Telken 5	0.696	0.002	0.947	0.001	0.937	0.004	0.989	0.005
Duplicates									
M3-U-M 2		0.671	0.002	0.955	0.001	0.964	0.006	1.009	0.006
M3-U-M 2 bis		0.711	0.002	0.955	0.001	0.962	0.004	1.006	0.005
TI-U-M 2		0.780	0.001	0.963	0.001	0.964	0.005	1.001	0.006